Infrared second-order optical susceptibility in InAs/GaAs self-assembled quantum dots

T. Brunhes, P. Boucaud,* and S. Sauvage

Institut d'Électronique Fondamentale, UMR CNRS 8622, Bâtiment 220, Université Paris-Sud, 91405 Orsay, France

A. Lemaître and J.-M. Gérard

France Telecom CNET, 196 Av. H. Ravera, 92225 Bagneux, France

F. Glotin, R. Prazeres, and J.-M. Ortega

CLIO/LURE, Bâtiment 209 D, Université Paris-Sud, 91405 Orsay, France

We have investigated the second-order nonlinear susceptibility in self-assembled quantum dots. The nonlinear susceptibility associated with intraband transitions in the conduction band and in the valence band is theoretically estimated for lens-shaped InAs/GaAs self-assembled quantum dots. The confined energy levels in the dots are calculated in the effective-mass approximation by solving the three-dimensional Schrödinger equation. Giant values of nonlinear susceptibility, about six orders of magnitude larger than the bull GaAs susceptibility, are predicted. We show that this enhancement results from three key features: (i) the achievement of the double resonance condition, (ii) the specific polarization selection rules of intraband transitions that allow both in-plane and z-polarized transitions with large dipole matrix elements to be optically active, and (iii) the small homogeneous linewidth of the intraband transitions. The conclusions of the calculations are supported by the measurement of the midinfrared nonlinear susceptibility in the valence band. The measurements have been performed using a picosecond free-electron laser. Both $\chi^{(2)}_{zzz}$ and $\chi^{(2)}_{zxx}$ components of the susceptibility tensor are observed. A satisfying agreement is found between theoretical and experimental values.

I. INTRODUCTION

Midinfrared second-order nonlinear susceptibilities in semiconductor heterostructures have attracted a strong interest in the recent years. Most of the work has been devoted to the nonlinearities associated with intersubband transitions in quantum wells. Two factors can explain the enhancement of the nonlinear susceptibility in two-dimensional heterostructures by comparison with bulk semiconductors: (i) the large dipole matrix elements associated with intersubband transitions;[1] (ii) the tailoring of the intersubband energies allowed by adjusting the quantum-well thicknesses. This feature allows the achievement of double resonance conditions (i.e., resonance between the energy of the pump and harmonic beams and the energy of the intersubband transitions) in asymmetric structures. The first demonstration of nonlinearity associated with intersubband transition was reported by Fejer *et al.*[2] with the observation of second-harmonic generation at a wavelength close to 10 μm. Many other nonlinearities have been later demonstrated, including third-harmonic generation[3] and optical rectification.[4] Most of the experimental demonstrations were obtained using intersubband transitions in the conduction band of GaAs- or InP-based quantum wells. One drawback of using the conduction-band intersubband transition is related to the polarization selection rule, which implies that only transitions polarized along the z growth axis are optically active. Shaw *et al.*[5] have considered the case of valence-band intersubband transitions where the polarization selection rule is relaxed because of valence-band mixing between heavy- and light-hole states. Although experimental evidence of second-harmonic generation has been reported, the nonlinear susceptibility was only slightly enhanced as compared to the bulk GaAs nonlinear susceptibility. Midinfrared second-harmonic generation has also been demonstrated in the valence band of SiGe/Si quantum wells,[6] but the involved intersubband transitions were z-polarized, as is the case for conduction-band intersubband transitions.

Semiconductor quantum dots appear as promising candidates to achieve large nonlinear susceptibilities. The quantum dots grown by the self-assembled growth technique have a naturally asymmetrical shape that provides the required symmetry breaking to observe second-order nonlinear susceptibility. By analogy with intersubband transitions, the dipole matrix elements associated with quantum-dot intraband transitions (also called intersublevel transitions in the literature) can be large, with typical dipole matrix element ranging from a fraction of a nanometer to a few nanometers.[7] However, the polarization selection rules for the quantum-dot intraband transitions differ from the polarization selection rules associated with intersubband transitions as a consequence of the three-dimensional potential confinement. Both in-plane polarized and z-polarized intraband transitions can be optically active in the conduction band and in the valence band of the quantum dots. This feature provides additional flexibility for realizing the resonance conditions, including the double resonance, between the pump and harmonic fields and the intraband transitions, which in turn leads to very large nonlinear susceptibilities in the midinfrared region. Moreover, it implies in turn that second-harmonic generation can be observed in quantum dots for a normal incidence light excitation. Another specific feature associated with the quantum dot is related to the optical coherence. In isolated three-dimensionally confined nanostructures with a δ-like density

PRB <u>61</u>   5562

of states, one expects the dephasing mechanisms to be dominated by the dephasing associated with energy relaxation.[8] The dephasing rate of the optical coherence is therefore given by $1/T_2 = \Gamma/2$, where Γ is the recombination rate associated with energy relaxation processes (i.e., phonon-assisted, Auger-mediated relaxation processes, etc.). Because of the slowing of the relaxation in quantum dots,[9] the lifetime-broadened intraband transitions are therefore expected to exhibit very narrow linewidths. Since, at double resonance, the second-order susceptibility is inversely proportional to the square of the homogeneous broadening, this feature can lead to very large values of the susceptibility. Note that this lifetime broadening mechanism is under debate. Li and Arakawa have suggested that in small quantum dots, the homogeneous linewidth is given by the lattice relaxation, i.e., the change of the lattice configuration induced by the different electronic states.[10]

The purpose of this paper is to show that record values of second-order nonlinear susceptibilities can be achieved using quantum-dot intraband transitions. To demonstrate this effect, the chosen model system corresponds to the standard Stranski-Krastanow InAs/GaAs self-assembled quantum dots.[11] Although the presented results are directly connected to the shape and composition of the quantum dots, similar features are expected to occur for other types or shapes of quantum dots. The quantum-dot energy levels are first calculated in the effective-mass approximation by solving the three-dimensional Schrödinger equation.[12] Then, the second-order nonlinear susceptibility is computed both in the conduction and in the valence band from the calculated energy dependence of the confined levels versus the quantum-dot size. A microscopic description, based on the allowed optical transitions, is given for the nonlinear optical processes. The angular dependence of the susceptibility is investigated. Giant nonlinear susceptibilities are predicted in the conduction band and in the valence band. This enhancement over the bulk response results from the achievement of resonance conditions with the intraband transitions polarized along different directions. The calculated susceptibility values are finally compared to the experimental values measured in the valence band of InAs/GaAs self-assembled quantum dots. The amplitude and the spectral dependence of the nonlinear susceptibility were measured with a free-electron laser. The angular dependence of the susceptibility was also investigated. A satisfying agreement with regard to amplitude, spectral dependence, and polarization is obtained between the theoretical and the experimental nonlinear susceptibilities. Experimentally, it is found that the amplitude of the nonlinear susceptibility of a single quantum-dot layer is enhanced by three orders of magnitude over the bulk GaAs nonlinear susceptibility. Although we could not observe the highest values of nonlinear susceptibilities that are predicted, the experimental observation of the second-order susceptibility for different polarizations gives strong support to our predictions.

The paper is organized as follows: Section II presents the energy-level calculation in the lens-shaped self-assembled quantum dots. The numerical simulations for the second-order nonlinear susceptibility are presented in Sec. III. The midinfrared nonlinear susceptibilities are evaluated for conduction- and valence-band intraband transitions. The dominant components of the susceptibility tensor are calculated as a function of the energy for various dot size distributions. The experimental measurement of the nonlinear susceptibility associated with valence-band intraband transitions is described in Sec. IV. The spectral dependence of the nonlinear susceptibility is investigated for two incident electric field polarizations. A comparison between the theoretical and experimental nonlinear susceptibilities is finally presented in Sec. V.

II. THEORY

A. Energy-level calculation

The calculation of confined energy levels in semiconductor quantum dots has been reported by several authors. Different methods have been applied to describe the energy states of self-assembled quantum dots, including single-band effective-mass calculation,[13–15] $\mathbf{k} \cdot \mathbf{p}$ calculations including multiple bands,[16–19] and pseudopotential theory.[20] The comparison between the energies predicted by these calculations and the experimental data is, however, limited by the exact knowledge of the quantum-dot shape, size, distribution, and composition. Although several methods, including cross-section transmission electronic microscopy or scanning tunneling microscopy[21] on cleaved edge, have been used to tackle these issues, some uncertainty remains on the exact quantum-dot shape, size, composition, and strain relaxation. Besides, the inhomogeneous broadening associated with the dot size distribution along with the dispersion observed from layer to layer in stacked structures usually limits the comparison accuracy between theoretical and experimental data.

In order to investigate the second-order nonlinear susceptibility associated with the intraband transitions, we have used a single-band effective-mass calculation to evaluate the energy of the confined levels as a function of the quantum-dot size. Though the effective-mass approach exhibits some significant deviation from more sophisticated calculations, previous studies have shown that this single-band model provides a coherent interpretation of the experimentally observed intraband transitions (polarization selection rule, dipole matrix elements).[22] We underline that the purpose of this article is to provide a guideline to predict the magnitude and polarization dependence of the second-order nonlinear susceptibilities in the quantum dots. An accurate description of the quantum-dot states and in particular of their energy, which would require a multiband $\mathbf{k} \cdot \mathbf{p}$ calculation or a pseudopotential calculation, is beyond the scope of this paper. Meanwhile, the accuracy of these calculations is intrinsically limited by the exact knowledge of the quantum-dot shape and composition. As will be shown below, a satisfying agreement is found between the experimental data and the theoretical predictions based on the single-band effective-mass approximation. This feature does not rule out a contribution of valence-band mixing effects to the nonlinear susceptibilities. Though beyond the scope of this paper, a comparison of the nonlinear susceptibilities predicted by the single-band model and $\mathbf{k} \cdot \mathbf{p}$ models would be interesting.

The average strain in the quantum-dot layer has been taken into account through band-offset and effective-mass modifications. In the conduction band, the band offset between InAs and GaAs is taken equal to 600 meV. In the
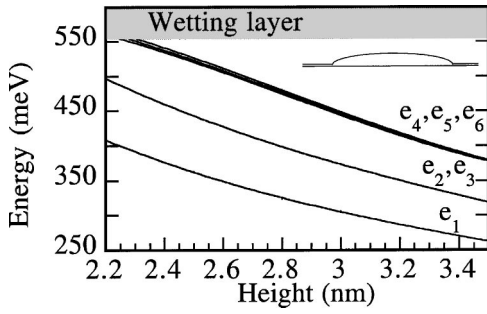
FIG. 1. Energy of the confined states in the conduction band as a function of the quantum-dot height. The aspect ratio (height/diameter) is kept constant and equal to 0.1. Above 560 meV, the confined states are hybridized with the wetting layer states. The two-dimensional wetting layer energy is found 40 meV below the GaAs conduction-band edge. The inset shows the quantum-dot geometry. Only the first six states are represented and some states are omitted for quantum-dot height larger than 3 nm.

valence band, the band offset is taken equal to 450 meV. The effective mass is considered as isotropic in the conduction band [$m_e = 0.04m_0$,[16] where m_0 is the bare electron mass], whereas it is decoupled between the z growth axis and the layer plane in the valence band ($m_z = 0.59m_0$, $m_{x,y} = 0.07m_0$).[12,22] Only the heavy-hole states are considered in the valence band, the light-hole states lying close the valence-band edge. The strain inhomogeneity has been ignored. The dipole matrix element d_{ij} for an intraband transition between state E_i (wave function ψ_i) and state E_j (wave function ψ_j) is defined as $d_{ij} = \langle \Psi_j | r | \Psi_i \rangle$. All the dipole matrix elements between the different transitions are calculated numerically.

The calculation is performed for a lens-shaped quantum-dot geometry that is close to the experimental geometry of the studied quantum dots as observed by transmission electron microscopy.[23] The quantum dot is defined as a truncated sphere cut by an horizontal plane. The quantum dot lies on a 0.5-nm two-dimensional (2D) layer, which corresponds to the InAs wetting layer. The quantum-dot parameters are given by the quantum-dot height h (distance between the bottom of the wetting layer and the top of the truncated sphere) and the quantum-dot diameter D. We have assumed a direct correlation between the quantum-dot height and the quantum-dot diameter. The single-particle energy levels are calculated as a function of the quantum-dot height for a fixed aspect ratio (height/diameter).

1. Conduction band

Figure 1 shows the confined energy states in the conduction band as a function of the quantum-dot height. For a typical quantum-dot height of 2.5 nm, only six levels are bound in the conduction band. Above 560 meV, the confined states are hybridized with the continuum associated with the two-dimensional wetting layer states. The ground state is an s-like state. The first excited state e_2 is doubly degenerate (p-like state) and results from the in-plane confinement. The e_4, e_5, e_6 states, which are very close in energy, also correspond to excited states associated with in-plane confinement.[24] The intraband transition between the ground and the first excited state is in-plane polarized (3.2 nm dipole

length) whereas the intraband transition involving the e_1 and e_6 states is z polarized (0.15 nm dipole length). This polarization selection rule is a consequence of the coupling between the z direction and the in-plane direction because of the lens-shaped geometry of the quantum dots. The same transition is forbidden in a cubic quantum box with infinite barrier potentials. The dipole matrix element between e_1 and e_4 or e_5 is zero. The first excited state e_2 has an in-plane dipole matrix element with the e_4, e_5, and e_6 states. It is worth noticing that for a 2.2-nm quantum-dot height, the intraband transition between the ground state to the wetting layer state is predicted at an energy close to 150 meV in agreement with the experimental transition energy.[25]

2. Valence band

The energies of the confined states in the valence band are shown in Fig. 2 as a function of the quantum-dot height. The number of confined states is much larger than that in the conduction band because of the heavier effective mass along the z direction. As for conduction-band intraband transitions, the largest dipole matrix element is associated with the h_1-h_2 transition (3.45 nm) and is oriented in the layer plane. Starting from the ground state, the next allowed transition is the h_1-h_4 transition with a 0.75-nm dipole matrix element along the z growth axis. The h_1-h_7 transition is z polarized with a 0.36-nm dipole matrix element. Experimentally, this transition is found to dominate the midinfrared absorption spectrum at energies larger than 90 meV. The h_1-h_8 transition is in-plane polarized with a 0.15 nm dipole length.
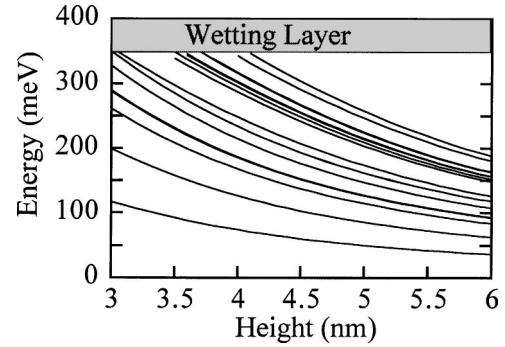

FIG. 2. Energy of the confined states in the valence band as a function of the quantum-dot height. The aspect ratio (height/diameter) is 0.2. The two-dimensional continuum wetting layer states are above 350 meV. Some states are not shown on the graph for quantum-dot heights larger than 5 nm.

III. SECOND-ORDER NONLINEAR SUSCEPTIBILITY

In order to calculate the second-order nonlinear susceptibility, we have assumed a Gaussian size distribution for the quantum dots. The width of this Gaussian σ is an adjustable parameter and can be fitted to the experimental data to reproduce the intraband absorption linewidth. The normalized quantum-dot distribution is given as a function of the quantum-dot height h by

$$D_\sigma(h) = \frac{1}{\sqrt{2\pi}\sigma} \exp[-(h-h_0)^2/2\sigma^2], \tag{1}$$

where h_0 is the average quantum-dot height. The second-order nonlinear susceptibility is calculated under the assumption that the intraband transitions are in close resonance with the incident pump excitation at an energy $\hbar\omega$. This situation corresponds to a condition where the double resonance (i.e., resonance of the pump and of the harmonic field with intraband transitions) can be achieved. Note that when the double resonance is not achieved (i.e., only a single resonance is satisfied), the susceptibility involves components that are proportional to the mean charge displacement.[26,27] These components were not considered in the following. Close to the double resonance, the dominant susceptibility $\chi^{(2)}_{kji}$ associated with the E_i-E_j and E_j-E_k intraband transitions can be written for a given quantum-dot height h:[28]

$$\chi^{(2)}_{kji}(h)$$

$$= \frac{e^3 N_{3D}}{\epsilon_0} \frac{\langle d_{ij}(h)\rangle \langle d_{jk}(h)\rangle \langle d_{ik}(h)\rangle}{[\hbar\omega - E_{ij}(h) - i\Gamma_{ij}][2\hbar\omega - E_{ik}(h) - i\Gamma_{ik}]}, \quad (2)$$

where e is the electronic charge and ϵ_0 the vacuum permittivity. N_{3D} is the three-dimensional carrier density in the quantum dots. The three-dimensional carrier density is obtained by dividing the equivalent 2D population of the dots by the thickness of the deposited InAs (two monolayers).[29] d_{ij} are the intraband dipole matrix elements corresponding to the E_i-E_j transition. These matrix elements can be oriented either in the layer plane or along the z direction. The dipole matrix elements, which exhibit a slight variation as a function of the quantum-dot height, are assumed to be constant. In the absence of experimental data, the homogeneous linewidth (half width at half maximum) Γ_{ij} of the different intraband transitions is taken constant in the following and equal to 0.2 meV.[30]

The quantum-dot susceptibility is integrated over the quantum-dot size distribution:

$$\chi^{(2)}_{kji} = \int_h \chi^{(2)}_{kji}(h) D_\sigma(h) dh. \quad (3)$$

The global susceptibility is summed over the different intraband transitions:

$$\chi^{(2)}_{2\omega} = \sum_{k,j,i=1} \chi^{(2)}_{kji}. \quad (4)$$

In the calculation, only the transitions starting from the ground state are considered, since, as experimentally observed, only this level is intentionally populated.

The components of the susceptibility tensor can be estimated for the different polarizations associated with the intraband transitions. In the following, we will restrict ourselves to the components that are experimentally observed and that are dominant, namely, $\chi^{(2)}_{zxx}$, $\chi^{(2)}_{zzz}$, and $\chi^{(2)}_{xxz}$. The parameters chosen for the calculation were deduced from the experimental data: the dot density was 4×10^{10} cm^{-2} and the doping density was 6×10^{10} cm^{-2}, either in the conduction or in the valence band. The susceptibility components involving the delocalized states in the continuum are not included in the calculation.
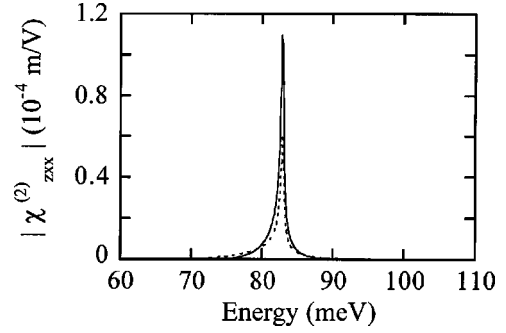

FIG. 3. Spectral dependence of the second-order nonlinear susceptibility $|\chi^{(2)}_{zxx}|$ calculated in the conduction band. Two distinct inhomogeneous broadenings are represented and correspond respectively to a 20% (dashed line) and a 10% (full line) dot size homogeneity. The average quantum-dot height is 2.5 nm.

A. Conduction-band susceptibility

The spectral dependence of the second-order nonlinear susceptibility associated with conduction-band intraband transitions is shown in Fig. 3. The average quantum-dot height is 2.5 nm. The susceptibility has been calculated for two different inhomogeneous broadenings, which correspond to a 20% and a 10% dot size fluctuation (full width at half maximum). These broadenings correspond to a 12- and a 7-meV linewidth for the e_1-e_2 intraband transition. Only the e_1-e_2 and e_1-e_6 transitions can be involved in the second-harmonic generation process since the dipole matrix element is zero between e_1 and e_4 or e_5. As mentioned above, the e_1-e_2 and the e_2-e_6 intraband transitions are in-plane polarized (3.2 nm dipole length). The e_1-e_6 transition is z polarized (0.15 nm dipole length). The corresponding susceptibility involving these transitions is therefore of the type $\chi^{(2)}_{zxx}$. As shown in Fig. 3, the nonlinear susceptibility is highly resonant with a sharp peak around 83 meV. The amplitude of the susceptibility increases as the inhomogeneous broadening is reduced because of a better homogeneity of the quantum-dot size distribution. The full width at half maximum of the susceptibility is similar in both cases. This broadening is determined by the energy dependence of the quantum-dot levels as a function of the quantum-dot size. The key feature, which is shown in Fig. 3, is the record value of the susceptibility that can be achieved for a reasonable inhomogeneous broadening of the quantum dots (10%). The susceptibility is predicted to be as high as 1×10^{-4} m/V, i.e., almost six orders of magnitude larger than the bulk GaAs value (1.9×10^{-10} m/V).[31] We underline that this calculated susceptibility is much larger than the highest susceptibilities reported so far for intersubband transitions in quantum wells. Two factors explain this enhancement over the bulk nonlinear susceptibility: (i) The double-resonance condition between e_1-e_2 and e_2-e_6 transitions is achieved for a quantum-dot height around 2.5 nm. This situation is the most favorable to achieve large nonlinear susceptibilities since the nonlinear coefficient is in this case inversely proportional to the square of the homogeneous broadening. (ii) The specific polarization selection rules of the quantum-dot intraband transitions are the second key parameter that explains the giant value of the susceptibility. For example, it is well known that in parabolic quantum wells, the double-
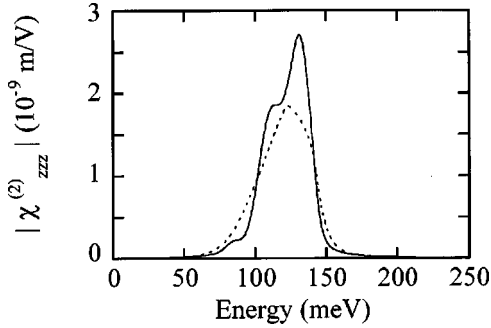
FIG. 4. Spectral dependence of the second-order nonlinear susceptibility $|\chi^{(2)}_{zzz}|$ calculated in the valence band. Two distinct inhomogeneous broadenings are represented and correspond, respectively, to a 20% (dashed line) and a 10% (full line) dot size homogeneity.

resonance condition is achieved; however, the nonlinear susceptibility vanishes since the dipole matrix element between the ground and the second excited state is strictly zero. In quantum dots, the situation is different: it is possible to achieve double-resonance conditions while keeping nonvanishing dipole matrix elements between the intraband transitions (dipole length in the nanometer range). This feature is a direct consequence of the three-dimensional potential confinement in the lens-shaped quantum dots. We emphasize that the highest value of the susceptibility can only be reached if the double-resonance condition is satisfied. Experimentally, this condition requires one to choose properly the average quantum-dot size that can satisfy this condition (2.5 nm height for the present lens-shaped quantum-dot geometry).

B. Valence-band susceptibility

In the valence band, the susceptibility has been calculated for quantum dots with an average height of 4.62 nm. This value is larger than that observed experimentally or than that used in the conduction band. However, a comparison between calculation and experimental data shows that the energy of the intraband transitions is overestimated in this single-band effective-mass model. In order to account for this effect, the quantum-dot average height has been adjusted to 4.62 nm in order to fit the h_1-h_7 intraband transition energy peak to the 110-meV value as experimentally observed.[30] In the following, only the main components of the susceptibility tensor are shown.

1. $\chi^{(2)}_{zzz}$

The spectral dependence of the nonlinear susceptibility $\chi^{(2)}_{zzz}$, which corresponds to z-polarized excitations, is presented in Fig. 4. Two different broadenings of the dot size distribution are considered (20% and 10% dot size fluctuation at full width at half maximum). These broadenings correspond to a 36- and a 20-meV linewidth for the h_1-h_7 transition. For a weak broadening, three resonances can be observed in the midinfrared region. The first peak at 87 meV is associated with the resonance of the harmonic pump with the h_1-h_{12} transitions; the second peak at 107 meV involves the h_1-h_7 intraband transitions. The third peak at 130 meV corresponds to the resonance between the second harmonic
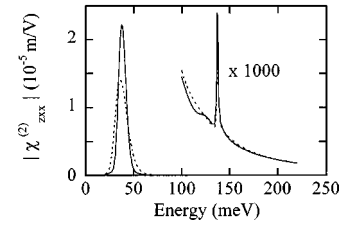

FIG. 5. Spectral dependence of the second-order nonlinear susceptibility $|\chi^{(2)}_{zxx}|$ calculated in the valence band. Two distinct inhomogeneous broadenings are represented and correspond respectively to a 20% (dashed line) and a 10% (full line) dot size homogeneity. The high-energy part of the graph has been multiplied by a factor of 1000.

and the h_1-h_{28} intraband transition. All the dominant microscopic mechanisms involve the z-polarized h_1-h_7 intraband transition. Since the double-resonance condition is not achieved for this polarization, the broadening of the susceptibility remains similar to the broadening of the absorption. Although the susceptibility remains higher than the bulk GaAs susceptibility, the magnitude of the nonlinear coefficient is much lower than that predicted in the conduction band.

2. $\chi^{(2)}_{zxx}$

The spectral dependence of the $\chi^{(2)}_{zxx}$ component of the nonlinear susceptibility is shown in Fig. 5 for two different quantum-dot distributions. This susceptibility component corresponds to an in-plane excitation while the second-harmonic polarization is oriented along the z growth axis. For these polarizations, the susceptibility is similar to that calculated in the conduction band. As expected, the susceptibility is dominated at low energy (37 meV) by the component that involves the transitions between the h_1, h_2, and h_4 states. The h_1-h_2 and h_2-h_4 transitions have the largest in-plane dipole matrix element (3.45 and 2 nm, respectively). Since the h_1-h_4 intraband transition is z-polarized, the susceptibility component is of the type $\chi^{(2)}_{zxx}$ as for the case of the conduction band. However, the double-resonance condition is not achieved for these transitions, which explains that the susceptibility remains significantly lower than that calculated in the conduction band. It is worth noticing that this susceptibility remains much larger than that reported in the valence band of quantum wells.[5] A narrow resonance is observed at higher energy (137 meV). This resonance involves the transitions between the h_1, h_8, and h_{29} states. The susceptibility value is enhanced in this case because of the double resonance between the pump, the harmonic field, and the intraband transitions. As will be shown below, this resonance has been observed experimentally. Smaller resonances can also be observed around 120 meV and are attributed to the resonance between the pump and the h_1-h_8 transition and the resonance between the harmonic field and the h_1-h_{12} transition.

3. $\chi^{(2)}_{xxz}$

The $\chi^{(2)}_{xxz}$ component of the susceptibility is reported in Fig. 6 for two quantum-dot size distributions. This component involves the z-polarized h_1-h_7 intraband transition, the

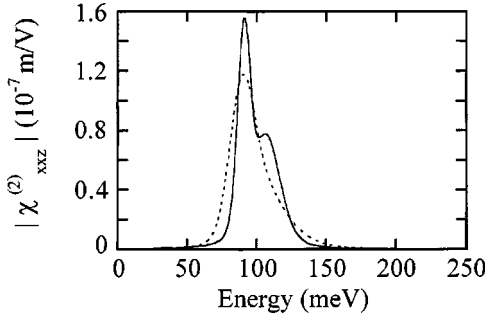FIG. 6. Spectral dependence of the second-order nonlinear susceptibility $|\chi^{(2)}_{xxz}|$ calculated in the valence band. Two distinct inhomogeneous broadenings are represented and correspond, respectively, to a 20% (dashed line) and a 10% (full line) dot size homogeneity.

in-plane polarized h_7-h_{13} transition and the in-plane polarized h_1-h_{13} transition as the final transition. The susceptibility exhibits two resonances at 91 and 110 meV. Since the double resonance is not achieved between these transitions, the two maxima reflect the resonance between the pump and the h_1-h_7 intraband transition and the resonance between the harmonic field and the h_1-h_{13} transition.

IV. EXPERIMENT

The experiments were performed using the free-electron laser CLIO. The free-electron laser delivers picosecond optical pulses that are widely tunable in the midinfrared spectral range. The output optical peak powers can be as high as 10 MW, which makes the free-electron laser a very convenient tool to study optical nonlinearities where both high intensities and tunabilities are required.

The investigated quantum-dot sample consists of 40 InAs quantum-dot layers grown by molecular beam epitaxy on GaAs. Details of the quantum-dot structure can be found in Ref. 30. Briefly, the quantum dots are separated by a 35-nm-thick GaAs layer. The quantum dots were grown in the core of a midinfrared waveguide grown on an n-doped GaAs substrate. The p-type quantum dots were modulation doped with boron. Since the dot densities is around $4 \times 10^{10} \, \mathrm{cm}^{-2}$ and the nominal doping density $6 \times 10^{10} \, \mathrm{cm}^{-2}$ one expects an average concentration of 1.5 carriers per dot.

In the midinfrared region (below 14 μm wavelength), the absorption spectrum of this sample is dominated by the h_1-h_7 intraband transition, which is polarized along the z growth axis of the quantum dots. The assignment of this absorption is made on the basis of a systematic study of the intraband transitions as a function of the quantum-dot size.[22] A weak h_1-h_{12} intraband transition is also observed at higher energy (160 meV). This transition is polarized in the quantum-dot layer plane. Third- and second-harmonic generations associated with intraband transitions have been successfully observed in this sample.[30,32] In the following, we focus on the second-harmonic generation with special attention devoted to the angular dependence of the nonlinear susceptibility.

The measurement was performed at room temperature. The infrared light was injected through the cleaved edge along the (110) direction of a 3-mm-long sample. The in-
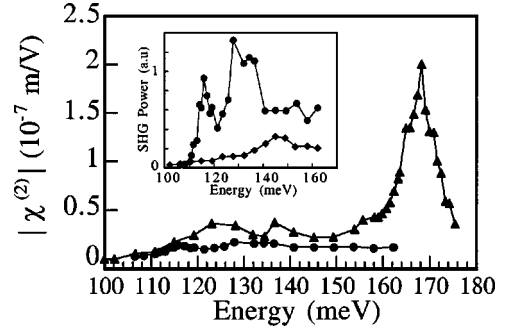

FIG. 7. Experimental spectral dependence of the second-order susceptibility measured for a TM-polarized (dots) and TE-polarized pump (triangles). The quantum dots are p-type doped. The susceptibility has been calibrated by reference to the bulk GaAs nonlinear susceptibility. The full curves are guides to the eyes. The inset shows a comparison of the spectral dependence of the second-harmonic power for the undoped (diamonds) and p-type doped (dots) quantum-dot sample (TM polarization).

coming polarization was set either in TM polarization (polarization along the z growth axis of the quantum dots) or in TE polarization (polarization along the quantum-dot layer plane), or it could be freely rotated. The measurement of the susceptibility amplitude was obtained by comparison with the second-harmonic signal generated by a reference sample with undoped quantum dots. In this case, only bulk GaAs (i.e., the nonzero $\chi^{(2)}_{zyx}$ susceptibility component) generates second-harmonic light. This comparison procedure is described in Ref. 32. The measured susceptibility corresponds to the susceptibility of the 40-dot layer planes averaged by the overlap factor of the dot planes with the optical mode. In order to extract the susceptibility of one layer plane, the global susceptibility is normalized by the 0.6% overlap factor between the quantum dots and the guided optical mode. This overlap factor is an important parameter, which limits the conversion efficiency. Although the quantum-dot susceptibility is very large, the global conversion efficiency associated with the quantum dots is only one order of magnitude larger than the one associated with bulk GaAs.[32]

The spectral dependence of the nonlinear susceptibility associated with intraband transitions is presented in Fig. 7. The vertical axis corresponds to the susceptibility of one quantum-dot layer. The susceptibility has been measured for two incident polarizations, TM (dots) and TE (triangles). Significant differences are observed between both curves. This feature is a direct consequence of the intraband transition polarization selection rules. The susceptibility is characterized by a resonant enhancement in TE polarization with a maximum at 168 meV. Such a narrow resonance is not observed in TM polarization. At peak maximum, the experimental susceptibility for one quantum-dot layer is as high as 2×10^{-7} m/V, which is three orders of magnitude larger than the bulk GaAs susceptibility. The full width at half maximum of this resonance is 7 meV. Two broader resonances are also observed in TE polarization at lower energy (125 and 136 meV). At these energies, the peak susceptibility is decreased by a factor of 5 as compared to the 168-meV peak susceptibility. Below 90 meV, the susceptibility could not be measured since the transmission of the sample vanishes be-

cause of the free-carrier absorption in the doped GaAs layers and the cutoff associated with the waveguide. It was therefore not possible to investigate the susceptibility at low energy.

In TM polarization, the susceptibility exhibits two maxima at 115 and 135 meV. It is worth noticing that the TM-polarized susceptibility, which corresponds to a z-polarized excitation, is much weaker than the TE-polarized susceptibility. We emphasize that no resonances are observed in this energy range for the reference sample with undoped quantum dots. This feature is shown in the inset of Fig. 7, which shows the spectral dependence of the second-harmonic power for the undoped and p-doped quantum-dot sample. The polarization of the harmonic signal was checked by inserting a polarizer behind the sample. The second harmonic was TM-polarized as evidenced by the cosine square dependence of the signal as a function of the polarizer angle.

We did not observe any saturation of the harmonic conversion in the investigated intensity range. The harmonic power exhibits a quadratic dependence with the pump intensity up to 200 MW cm^{-2}. It is worth noting that some of the dipole matrix elements involved in the harmonic-generation process are weak (0.1 nm or less). An accurate study of the second-harmonic generation saturation in quantum dots would require a nonperturbative approach, which accounts for the population saturation, the ac Stark splitting of the levels, and the detuning of the transitions from the resonance.[33]

V. COMPARISON BETWEEN THEORY AND EXPERIMENT

The amplitude and the spectral dependence of the quantum-dot susceptibility in TE and TM polarizations can be compared to the calculated values. The purpose of this comparison is not to find a perfect agreement between the energy maxima. In the valence band, this feature is ruled out by the simplicity of the energy-level calculation. Nonetheless, as shown below, a qualitative agreement can be found on the absolute magnitude of the susceptibility along with an agreement on the ratio between the polarized components of the susceptibility.

The comparison between the TM component of the susceptibility and the $\chi^{(2)}_{zzz}$ value is shown in Fig. 8. $\chi^{(2)}_{zzz}$ represents the largest component of the susceptibility for a z-polarized incident excitation. For the calculation, the quantum-dot size is considered to fluctuate by 10% around the 4.6 nm height. A satisfying agreement is obtained for the spectral shape between both curves. The experimental amplitude of the susceptibility is found larger by one order of magnitude as compared to the theoretical susceptibility. We emphasize that the calculated value is strongly dependent on the values of the dipole matrix elements, on homogeneous broadening, and on the exact numbers of carriers that are involved in the second-harmonic generation process. A discrepancy by a factor of 10 remains therefore reasonable in view of the uncertainty on these parameters. The narrow resonance at 115 meV is related to nonlinear processes that involve the h_1-h_7 intraband transition. The broader component, which has a peak at 135 meV, is attributed to transi-
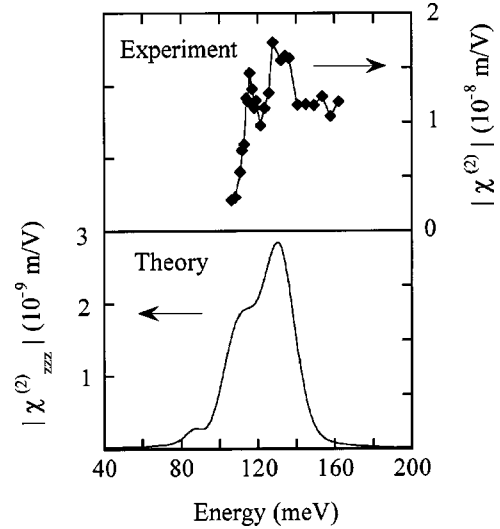

FIG. 8. Comparison between the susceptibility measured in TM polarization for p-type doped quantum dots and the second-order nonlinear susceptibility $|\chi^{(2)}_{zzz}|$ calculated in the valence band (10% dot size homogeneity). Note the two different vertical scales.

tions that involve the h_1-h_{28} intraband transition.

The comparison between the experimental susceptibility measured for a TE excitation and the $\chi^{(2)}_{zxx}$ calculated value is shown in Fig. 9. Again, $\chi^{(2)}_{zxx}$ features the largest component of the susceptibility tensor for an in-plane excitation. The calculated susceptibility does not account for the susceptibility associated with the h_1, h_2, and h_4 states, which exhibits a broad tail towards high energy (Fig. 5). Experimentally, no signature of this broad tail has been observed. This feature is explained by the fact that the h_1-h_2 transition is resonant at an energy that is lower than the calculated one.[34] The resonant peak at 168 meV is attributed to the resonant process involving the h_1-h_8 and h_1-h_{29} intraband transitions. This resonance is also observed in the theoretical susceptibility at

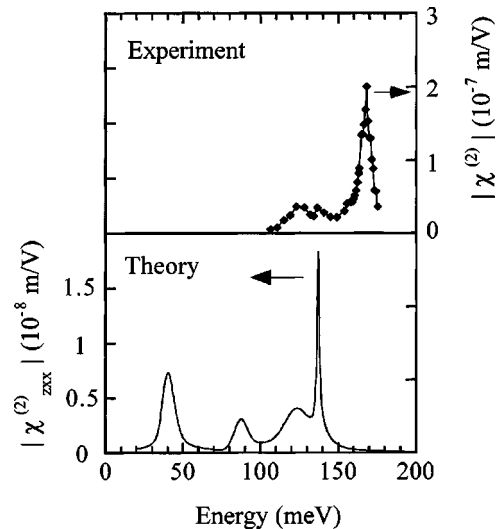FIG. 9. Comparison between the quantum-dot susceptibility measured in TE polarization and the second-order nonlinear susceptibility $|\chi^{(2)}_{zxx}|$ calculated in the valence band (10% dot size homogeneity). Note the two different vertical scales.

a lower energy (137 meV). The discrepancy between these two values is explained by the fact that for the present set of parameters (quantum-dot diameter, geometry, in-plane effective mass,. etc.), the h_1-h_8 transition is predicted to occur at 140 meV, whereas it is experimentally observed at 160 meV. Nonetheless, the comparison between theoretical and experimental susceptibility is a direct demonstration that double-resonant second-harmonic generation has been achieved in the quantum dots. As for the case of TM polarization, a discrepancy (factor of 10) between the experimental and the theoretical amplitudes is observed. This discrepancy originates mainly from an underestimation of the dipole matrix elements, which is more pronounced for the levels lying close to the wetting layer and from an overestimation of the homogeneous broadening.

We can also observe that the calculated susceptibility that corresponds to the TE excitation remains higher than the $\chi^{(2)}_{zzz}$ susceptibility. A comparison between the susceptibilities measured in TM and TE polarizations shows a similar behavior.

At this stage, it is worth noting that nonlinear optics are being used to investigate the electronic structure of quantum dots. Although the number of confined states is large, only a limited number of intraband transitions contribute significantly to the nonlinear susceptibility. It is also worth noticing that a single-band effective-mass model that accounts for the quantum-dot geometry gives a satisfying description of the confined energy states for interpreting the nonlinear experimental data.

VI. CONCLUSION

In conclusion, we have presented a theoretical calculation of the second-order nonlinear susceptibility associated with intraband transitions in self-assembled quantum dots. The quantum-dot energy levels have been calculated by solving the three-dimensional Schrödinger equation for a quantum-dot lens-shaped geometry. Both conduction- and valence-band susceptibilities have been investigated. Giant values of the susceptibility were predicted in the midinfrared spectral range. This enhancement over the bulk susceptibility results from the nanometer-scale dipole matrix elements of the intraband transitions and the achievement of double resonance condition between the pump, the harmonic, and the intraband transitions. Since in-plane polarized and z-polarized intraband transitions are allowed in quantum dots, the second-order susceptibility is not only restricted to z-polarized components, as is the case for intersubband transitions in the conduction band of quantum wells. The calculations are supported by the experimental measurement of the susceptibility in the midinfrared region for TM- and TE-polarized excitations. A satisfying agreement is observed between the experimental and theoretical values. This work shows that quantum dots and in particular self-assembled quantum dots are good candidates to obtain record values of nonlinear susceptibilities.

*Present address: Dept. of Physics, Quantum Institute, University of California, Santa Barbara, CA 93106-9530. Electronic address: boucaud@qi.ucsb.edu

[1] L. C. West and S. J. Eglash, Appl. Phys. Lett. **46**, 1156 (1986).

[2] M. M. Fejer, J. J. B. Yoo, R. L. Byer, A. Harwitt, and J. S. Harris, Jr., Phys. Rev. Lett. **62**, 1041 (1989).

[3] C. Sirtori, F. Capasso, D. L. Sivco, and A. Y. Cho, Phys. Rev. Lett. **68**, 1010 (1992).

[4] E. Rosencher, A. Fiore, B. Vinter, V. Berger, Ph. Bois, and J. Nagle, Science **271**, 168 (1996).

[5] M. J. Shaw, M. Jaros, Z. Xu, P. M. Fauchet, C. W. Rella, B. A. Richman, H. A. Schwettman, and G. W. Wicks, Phys. Rev. B **50**, 18 395 (1994).

[6] M. Seto, M. Helm, Z. Moussa, P. Boucaud, F. H. Julien, J.-M. Lourtioz, F. Nützel, and G. Abstreiter, Appl. Phys. Lett. **65**, 2969 (1994).

[7] H. Drexler, D. Leonard, W. Hansen, J. P. Kotthaus, and P. M. Petroff, Phys. Rev. Lett. **73**, 2252 (1994).

[8] N. H. Bonadeo, G. Chen, D. Gammon, D. S. Katzer, D. Park, and D. G. Steel, Phys. Rev. Lett. **81**, 2759 (1998).

[9] H. Benisty, C. M. Sottomayor-Torrès, and C. Weisbuch, Phys. Rev. B **44**, 10 945 (1991).

[10] X-Qi. Li and Y. Arakawa, Phys. Rev. B **60**, 1915 (1999).

[11] L. Goldstein, F. Glas, J. Y. Marzin, M. N. Charasse, and G. Le Roux, Appl. Phys. Lett. **47**, 1099 (1985).

[12] S. Sauvage, P. Boucaud, J.-M. Gérard, and V. Thierry-Mieg, Phys. Rev. B **58**, 10 562 (1998).

[13] J.-Y. Marzin and G. Bastard, Solid State Commun. **92**, 437 (1994).

[14] M. Grundmann, O. Stier, and D. Bimberg, Phys. Rev. B **52**, 11 969 (1995).

[15] L. R. C. Fonseca, J. L. Jimenez, J. P. Leburton, and R. M. Martin, Phys. Rev. B **57**, 4017 (1998).

[16] M. A. Cusack, P. R. Briddon, and M. Jaros, Phys. Rev. B **54**, R2300 (1996).

[17] H. Jiang and J. Singh, Phys. Rev. B **56**, 4696 (1997).

[18] C. Pryor, Phys. Rev. B **57**, 7190 (1998).

[19] O. Stier, M. Grundmann, and D. Bimberg, Phys. Rev. B **59**, 5688 (1999).

[20] J. Kim, L.-W. Wang, and A. Zunger, Phys. Rev. B **57**, R9408 (1998).

[21] B. Legrand, B. Grandidier, J. P. Nys, D. Stievenard, J. M. Gérard, and V. Thierry-Mieg, Appl. Phys. Lett. **73**, 96 (1998).

[22] S. Sauvage, P. Boucaud, J.-M. Gérard, and V. Thierry-Mieg, Phys. Rev. B **58**, 10 562 (1998).

[23] J. M. Gérard, J. Y. Marzin, G. Zimmermann, A. Ponchet, O. Cabrol, D. Barrier, B. Jusserand, and B. Sermage, Solid-State Electron. **40**, 807 (1996).

[24] The states can also be classified by reference to the parallelepipedal quantum dot with infinite barriers, where the states are classified according to the number of nodes of the eigenfunction along the x, y, and z directions. The levels e_4, e_5, and e_6 would correspond in this notation to e_{200}, e_{020}, and e_{110}, respectively. In a similar way, h_4 corresponds to h_{110} and h_7 to h_{001}.

[25] S. Sauvage, P. Boucaud, F. Glotin, R. Prazeres, J. M. Ortega, A. Lemaître, J. M. Gérard, and V. Thierry-Mieg, Appl. Phys. Lett. **73**, 3818 (1998).

[26] E. Rosencher and P. Bois, Phys. Rev. B **44**, 11 315 (1991).

[27] J. N. Heyman, K. Craig, B. Galdrikian, M. S. Sherwin, K. Campmann, P. F. Hopkins, S. Fafard, and A. C. Gossard, Phys. Rev. Lett. **72**, 2183 (1994).

[28] Y. R. Shen, *The Principles of Nonlinear Optics* (Wiley, New York, 1984).

[29] In this paper, the second-order nonlinear susceptibility in m/V is calculated with an equivalent three-dimensional carrier density. This procedure has also been used in quantum wells. A two-dimensional carrier density could, however, be used for comparison purposes between quantum wells and quantum dots. Note that the growth kinetic limits the stacking of quantum-dot layers. Isolated quantum dots require a distance of at least 5 nm between the wetting layers. This thickness could also be used to obtain a three-dimensional carrier density.

[30] S. Sauvage, P. Boucaud, F. Glotin, R. Prazeres, J.-M. Ortega, A. Lemaître, J. M. Gérard, and V. Thierry-Mieg, Phys. Rev. B **59**, 9830 (1999).

[31] Z. H. Levine and D. C. Allan, Phys. Rev. Lett. **66**, 42 (1991).

[32] T. Brunhes, P. Boucaud, S. Sauvage, F. Glotin, R. Prazeres, J. M. Ortega, A. Lemaître, and J. M. Gérard, Appl. Phys. Lett. **75**, 835 (1999).

[33] T. A. DeTemple, L. A. Bahler, and J. Osmundsen, Phys. Rev. A **24**, 1950 (1981).

[34] S. Sauvage, P. Boucaud, T. Brunhes, A. Lemaître, and J. M. Gérard, Phys. Rev. B **60**, 15 589 (1999).